

Galactic rotation curves, the baryon-to-dark-halo-mass relation and space–time scale invariance

Xufen Wu^{1,*}, Pavel Kroupa^{2,*}

¹ Department of Astronomy, University of Science and Technology of China, Jinzai Road 96, 230026, Hefei, China

² Helmholtz-Institut für Strahlen-und Kernphysik, Universität Bonn, Nussallee 14-16, D-53115 Bonn, Germany

* Email: xwu@astro.uni-bonn.de; pavel@astro.uni-bonn.de

27 October 2014

ABSTRACT

Low-acceleration space–time scale invariant dynamics (SID, Milgrom 2009a) predicts two fundamental correlations known from observational galactic dynamics: the baryonic Tully-Fisher relation (BTFR) and a correlation between the observed mass discrepancy and acceleration (MDA) in the low acceleration regime for disc galaxies. SID corresponds to the deep MODified Newtonian Dynammics (MOND) limit. The MDA data emerging in cold/warm dark matter (C/WDM) cosmological simulations disagree significantly with the tight MDA correlation of the observed galaxies. Therefore, the most modern simulated disc galaxies, which are delicately selected to have a quiet merging history in a standard dark-matter-cosmological model, still do not represent the correct rotation curves. Also, the observed tight correlation contradicts the postulated stochastic formation of galaxies in low-mass DM haloes. Moreover, we find that SID predicts a baryonic to apparent virial halo (dark matter) mass relation which agrees well with the correlation deduced observationally assuming Newtonian dynamics to be valid, while the baryonic to halo mass relation predicted from CDM models does not. The distribution of the observed ratios of dark-matter halo masses to baryonic masses may be empirical evidence for the external field effect, which is predicted in SID as a consequence of the forces acting between two galaxies depending on the position and mass of a third galaxy. Applying the external field effect, we predict the masses of galaxies in the proximity of the dwarf galaxies in the Miller et al. sample. Classical non-relativistic gravitational dynamics is thus best described as being Milgromian, rather than Newtonian.

Key words: gravitation – galaxies: general – galaxies: stellar content – galaxies: kinematics and dynamics

1 INTRODUCTION

The currently widely accepted understanding of gravity is based entirely on the empirical law derived by Newton. Newton based his derivation on a number of observations, the central ones being the laws of planetary motion proposed by Kepler. Einstein (1916) revolutionized our concept of gravitation as being not a force but an effect due to space–time curvature. Einstein’s field equation is in turn based on Newton’s law derived on the Solar System scale: at the time of Einstein’s proposal in 1916, galaxies had not been discovered to be what we know them to be nowadays. Thus, when applied to galaxies and cosmological scales, the Einsteinian/Newtonian law of gravity constitutes an extrapolation by many orders of magnitude in spatial and acceleration scale beyond the gravitational systems known in 1916. The observation that the rotation curves of galaxies

deviate from the expected Keplerian decline by being essentially flat at large radii, r (Rubin & Ford 1970; Bosma 1981; Rubin et al. 1982), i.e. that the circular velocities of galaxies obey $v_{circ} \approx \text{constant}$, is therefore a very major discovery. This behavior violates Newton’s empirical law of gravity that predicts a Keplerian fall off of the circular velocity, $v_{circ} \propto r^{-1/2}$, in the outer regimes of galaxies. It is not entirely surprising that Einsteinian/Newtonian gravity breaks down at those scales. However, today the popular interpretation of this discrepancy is to assume Newtonian/Einsteinian gravitation to be valid and to postulate the existence of cold (C) or warm (W) dark matter (DM) particles which make up the mass-discrepancy when rotation curves are interpreted in terms of Einsteinian/Newtonian gravitation. However there exists no experimental evidence for the existence of additional (e.g., dark matter) particles

beyond those predicted or contained within the standard model of particle physics despite a highly significant effort for finding them (see e.g. the recent press release from the direct search for dark matter particles with the Large Underground Xenon dark matter detector, Akerib et al. 2013; Kroupa 2014). Therefore it is important to test alternative gravities, amongst which Milgromian dynamics¹ (Milgrom 1983c) is the most promising one.

On the scale of galaxies, a mass-discrepancy–acceleration (MDA) correlation has been predicted by Milgrom (1983c): there is an exact correlation between the mass discrepancy (i.e., the amount of unseen additional mass needed when interpreting the observed motions within the Newtonian dynamics framework) and the acceleration deduced from the orbits at all radii observed in galaxies. The mass discrepancy, $\frac{M_{dyn}(<r)}{M_b(<r)} \propto \left[\frac{v(r)}{v_b(r)} \right]^2$, since it is well known that

$$v(r)^2 \equiv g(r)r \simeq \frac{GM_{dyn}(<r)}{r}, \quad (1)$$

$$v_b(r)^2 \equiv g_N(r)r \simeq \frac{GM_b(<r)}{r}, \quad (2)$$

where $M_{dyn}(<r)$ is the dynamical mass (i.e., the total Newtonian mass) within r , $v(r)$ is the total observed or actual rotation speed at r , $v_b(r)$ is the rotation speed at r contributed only from the baryons assuming Newtonian dynamics (note that “ \simeq ” in Eqs. 1-2 becomes an equality when the system is spherically symmetric).

This MDA correlation has been quantified empirically by Sanders (1990) and more recently by McGaugh (2004) for a sample of 74 disc galaxies. This correlation is extended to the Solar System scale by Famaey & McGaugh (2012, their fig. 4). Trippe (2013) fitted the MDA relation using McGaugh (2004) data in a massive graviton model, which is equivalent to MOND with a simple interpolating function. Scarpa (2006) tested this correlation for a sample of over 1000 pressure-supported systems from globular clusters to rich clusters of galaxies. More precisely, Scarpa (2006) studied the correlation between g and g_N instead of the MDA correlation. However, these two correlations, though formally different, are fully equivalent. Tiret & Combes (2009) examined the MDA correlation for a sample of 43 galaxies including early- and late-type galaxies.

The prediction by Milgrom (1983c) of the MDA correlation and its subsequent empirical confirmation offer detailed tests of theories of galaxy formation and dynamics. One of the major questions addressed with this contribution is whether galaxies simulated in the W/CDM cosmological frameworks also reproduce the observed MDA correlation. This is a timely question to ask, because recently there have been claims that disc galaxies can form in the DM models and that these galaxies also resemble real galaxies.

Noteworthy is that the deep Milgromian limit (i.e., dynamics in the weak field regime where $g \ll a_0$; here Milgrom’s constant $a_0 \approx 1.2 \times 10^{-10} \text{ m/s}^2$) can be derived

from space–time scale invariance and appears to be a constant of nature) can be described extremely well with low-acceleration space–time scale-invariant dynamics (hereafter SID, Sec. 2), as originally pointed out by Milgrom (2009a). With this contribution we revisit pure SID. It is shown, using simple arguments, how phantom (i.e. unreal) dark matter haloes, the BTFR and the MDA correlation emerge naturally within SID for an observer who interprets observations in terms of Newtonian dynamics. Therewith this further affirms the Milgrom’s and Bekenstein’s extension of effective gravity beyond the 1916 version as being realistic, in contrast to the introduction of C/WDM particles which are speculated to exist outside the standard model of physics.

The Strong Equivalence Principle (SEP) is violated in SID because of external fields (Milgrom 1983c; Bekenstein & Milgrom 1984). This violation is a direct outcome of the truncation of the phantom dark matter haloes as can be demonstrated nicely in the pure SID regime. *This means that in SID, the force acting between two galaxies depends on the position and mass of a third galaxy.* The violation of SEP is one of the most fundamental differences between SID/MOND and W/CDM. The violation of the SEP means that SID/MOND cannot be obtained by taking the non-relativistic limit of Einstein’s GR, which is known to be built on the basis of SEP. The internal dynamics of a system embedded in an external field depends on both the internal and the external gravitational fields (Milgrom 1983c; Bekenstein & Milgrom 1984). Therefore, it is important to study the effects of the external fields for real galaxies embedded in clusters of galaxies, and of satellite galaxies, to improve our constraints on the validity of SID and thus of Milgromian dynamics.

SID is discussed in Sec. 2. The MDA correlation is shown to directly and immediately emerge from SID. The connection between SID and MOND is discussed in Appendix A. We then visit in Sec. 3 the standard interpretation of the MDA correlation in terms of C/WDM and consult the most advanced astrophysical models of disc galaxy formation, which claim to explain disc galaxies readily. The baryonic-to-dark-matter-halo mass relation is studied in Sec. 4 for the SID prediction and for the C/WDM simulations, and a comparison to the observations is provided. The external field effect predicts a truncation of the phantom dark matter haloes in SID. This is studied in Sec. 4.3, where possible observational evidence for this important truncation is documented. We conclude with Sec. 5.

2 SPACE–TIME SCALE INVARIANT DYNAMICS AND THE MDA CORRELATION

In this section we revisit low-acceleration space–time scale-invariant dynamics (SID) raised by Milgrom (2009a) concerning the deep-MOND limit. The reader is reminded that most of the universe is in the SID regime (Kroupa 2014). It is also shown that in the low acceleration regime the MDA correlation follows from SID and the BTFR also immediately follows from SID. We thereby stress again that is a remarkable fact that such a simple symmetry, discovered by Milgrom (2009a), leads to such profound and correct reproduction of the most important laws of observed galactic

¹ Milgromian dynamics, often referred to as Modified Newtonian Dynamics (MOND), is briefly introduced in Appendix A, but here focus is on the deep-MOND or weak-acceleration limit, which is the regime of scale-invariant dynamics (SID, Sec. 2).

dynamics. It also follows from SID using simple arguments that apparent (i.e. non-particle) ‘dark matter haloes’ arise simply and directly, as is shown in sec. 2.1 in Wu & Kroupa (2013) and this is applied to the external field effect in Sec. 4.2–4.3.1 to demonstrate that the effective gravitating masses of galaxies depend on the position and mass of neighboring galaxies.

Consider a space–time scale invariance of the equations of motion under the consideration of the transformation in Minkowsky space (Milgrom 2009a; see also Milgrom 2014b,a),

$$(t, \mathbf{r}) \rightarrow (\lambda t, \lambda \mathbf{r}), \quad (3)$$

where t and $\mathbf{r} = (x, y, z)$ are time and Cartesian coordinates, respectively, and λ is a positive number. The Newtonian gravitational acceleration for a spherically symmetric system,

$$g_N = \frac{GM_b}{r^2}, \quad (4)$$

then transforms as $g_N \rightarrow \lambda^{-2} g_N$, whereas the kinematical acceleration, $g \equiv dx/dt$, scales as $g \rightarrow \lambda^{-1} g$. Here $M_b(< r)$ is the enclosed baryonic mass within r . As a result, the Newtonian gravitational acceleration and the kinematical acceleration scale differently under Eq. 3. Linking purely gravitational interactions to symmetries such as defined in Eq. 3 suggests deeper physics and constitutes a motivation for viewing MOND as much more than a mere phenomenological description of galactic dynamics (Milgrom 2009c). In order to assure that both, the gravitational and the kinematical accelerations scale symmetrically under Eq. 3, that is, in order to maintain the invariant symmetry, the gravitational acceleration, g , has to scale proportionally to $g_N^{1/2}$. In order to obtain the correct dimension, a constant with the unit of acceleration, needs to be introduced. This constant is referred to as a_0 , such that

$$g = (a_0 g_N)^{1/2}, \quad (5)$$

i.e. $g^2 = a_0 g_N$. Thus $g = (GM_b a_0)^{1/2}/r$, and the circular velocity, which follows from the centrifugal acceleration $g = v^2/r$, is

$$v = (GM_b a_0)^{1/4} = \text{constant}, \quad (6)$$

which is exactly the BTFR (Milgrom 1983c; McGaugh et al. 2000; Milgrom 2009a; Famaey & McGaugh 2012; Milgrom 2014b). We refer to gravitational dynamics which thus conforms to low-acceleration scale-invariance (Eq. 3) as low-acceleration scale-invariant dynamics (SID). SID beautifully reproduces the deep MOND equations of motion. It is rather remarkable that such a simple principle as SID and discovered by Milgrom leads to one of the most important scaling relations which real galaxies are observed to obey. Note that Eq. 6 implies that each baryonic galaxy is surrounded by a logarithmic non-particle (and thus phantom) dark matter halo potential, which is however not a real halo as it is only evident if Newtonian dynamics is applied to the galaxy. If SID is true, then a Newtonian observer would thus deduce that each baryonic galaxy is surrounded by a phantom DM

halo the mass of which is proportional to radial distance (Eq. 27 below).

Under SID and due to Eq. 1–2, for a spherical system, the mass discrepancy,

$$\left(\frac{v}{v_b} \right)^2 = \frac{g}{r} \cdot \frac{r}{g_N} = \frac{g}{g_N}, \quad (7)$$

becomes $\frac{(GM_b a_0)^{1/2}}{GM_b/r} = \left(\frac{a_0}{g_N} \right)^{1/2}$. Thus SID immediately implies a simple relation between the mass discrepancy and the baryonic Newtonian acceleration under the invariance transformation,

$$\left(\frac{v}{v_b} \right)^2 = \left(\frac{a_0}{g_N} \right)^{1/2}. \quad (8)$$

This function (Eq. 8) is plotted in the upper panel of Fig 1, where it is compared with the observational data in the weak-field regime ($g_N < 0.2 \times 10^{-10} \text{ m/s}^2$). The lower panel of this figure also shows the observationally deduced acceleration, g , in dependence of g_N . A value for a_0 can be obtained by fitting Eq. 8 to the data points in Fig. 1 (cyan curve). A Levenberg–Marquardt fit to the observed MDA data is shown in the upper panel of Fig. 1. *It follows that pure SID constitutes an excellent description of the observational data for $a_0 = 1.24 \pm 0.03 \times 10^{-10} \text{ m s}^{-2} = 3.90 \pm 0.01 \text{ pc Myr}^{-2}$ (within 1σ confidence level) for data points within the above mentioned weak field regime.*

SID is broken near gravitating masses whenever g approaches a_0 from below such that gravitational dynamics becomes Newtonian. A connection between the Newtonian regime and the SID regime is required to study the kinematic acceleration in the transitional regime where $g \simeq a_0$. To study the kinematics of galaxies in the full regime of acceleration, a transition function μ is introduced by Milgrom (1983c), yielding the full MOND description of galactic dynamics (Appendix A). The kinematic acceleration, \mathbf{g} , is transformed from the Newtonian acceleration, \mathbf{g}_N , through

$$\mathbf{g}_N = \mu(|\mathbf{g}|/a_0) \mathbf{g}, \quad (9)$$

with the help of the $\mu(|\mathbf{g}|/a_0)$ function.² Several forms of the $\mu(|\mathbf{g}|/a_0)$ function have been proposed by Milgrom (1983c, 1999) and Bekenstein (2004); Famaey & Binney (2005); Zhao (2008). We use two of the most popular interpolating functions: the ‘simple’ μ -function and the ‘standard’ μ -function,

$$\begin{aligned} \mu(x) &= \frac{x}{1+x}, & \text{‘simple’ } \mu, \\ \mu(x) &= \frac{x}{\sqrt{1+x^2}}, & \text{‘standard’ } \mu, \\ x &\equiv |\mathbf{g}|/a_0. \end{aligned} \quad (10)$$

² Note that this is, from the procedural point of view, equivalent to Planck (1901) introducing the constant \hbar as an auxiliary constant (“Hilfsgröße” in German) to describe the transition between the low-energy Rayleigh–Jeans black body spectrum and the downturn towards high-energies observed for black body radiators. The quantisation of energy had not been realised to be the underlying physics until more than 25 years later.

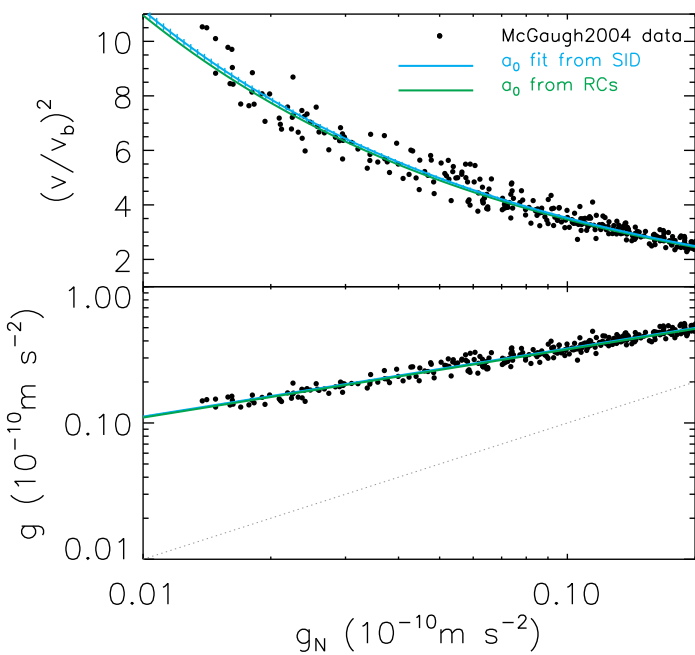


Figure 1. Upper panel: The mass discrepancy $(v/v_b)^2$ versus baryonic acceleration g_N in the weak field ($g_N < 0.2a_0 \ll a_0$) regime. The black points are the observed mass-discrepancy-baryonic-acceleration data by McGaugh (2004), and the cyan curve is the best fit of the MDA correlation for these data (see Eq. 8), where $a_0 = 1.24 \times 10^{-10} m s^{-2}$. The green curve is the MDA correlation with a_0 determined from observations of galactic rotation curves (see Sec. 2, Begeman et al. 1991). Lower panel: the kinematical acceleration versus Newtonian gravitational acceleration in the weak field regime. The observed data show a tight correlation between g and g_N . The faint dotted line shows the $g = g_N$ relation, which is not followed by the observational data.

We note here that the complete Milgromian description of classical gravity has been shown to have a Lagrangian formulation (Bekenstein & Milgrom 1984) such that this theory is energy and angular momentum conserving. For a spherically symmetric, cylindrically symmetric or axi-symmetric system, the solution of the Lagrangian formulation takes the simplified form, Eq. 9 (Bekenstein & Milgrom 1984). The standard form of the μ -function can be associated with quantum mechanical processes in the vacuum (Milgrom 1999, see also Appendix A in Kroupa et al. 2010).

Thus a relation between the mass discrepancy and the acceleration over the full classical regime is determined by the interpolating μ -function:

$$\left(\frac{v}{v_b}\right)^2 = \frac{g \cdot r}{g_N \cdot r} \simeq \frac{1}{\mu(x)}. \quad (11)$$

This indicates that the formation of galaxies cannot be stochastic, since otherwise the observational MDA data would have a much wider spread. The MDA correlation conflicts with the requirement of Λ CDM cosmological simulations that galaxy formation in low-mass DM haloes must be stochastic (Boylan-Kolchin et al. 2011). In such a speculative stochastic galaxy formation model, the C/WDM halo

mass ceases to be correlated with its baryonic/luminous galaxy. A further discussion of the MDA correlation for Λ CDM-simulated galaxies can be found in Sec. 3. More quantitative studies of the different forms of the μ -function will also be presented in Sec. 3.

3 STANDARD COSMOLOGICAL MODELS AND THE MDA CORRELATION

Despite the observations indicating rather convincingly that gravitation in the classical regime is Milgromian (Sec. 2), it is more popular to describe galactic dynamics by postulating Newtonian gravity to be valid as a major extrapolation from the Solar System scale to the scale of galaxies plus the existence of dynamically significant C/WDM particles which are neither described by nor contained within the otherwise highly successful standard model of particle physics (Blumenthal et al. 1984; Davis et al. 1985). The resulting standard cosmological model, the AC/WDM model, has been subject to significant testing (Kroupa et al. 2010; Kroupa 2012, 2014). One of the major problems for the Λ CDM model is that the merging history of each major dark matter halo makes the formation of disc galaxies highly problematical and until now not convincingly successful.

In the past two decades, the formation of disc galaxies has been extensively investigated by means of standard Λ CDM cosmological simulations (Katz & Gunn 1991; Navarro & Benz 1991; Navarro & Steinmetz 1997; Weil et al. 1998; Abadi et al. 2003; Piontek & Steinmetz 2011; Hummels & Bryan 2012; Agertz et al. 2011; Guedes et al. 2011; Aumer et al. 2013; Marinacci et al. 2013). The rotation curve has attracted particular interest since it is one of the most important tools to examine the reality of the simulated disc galaxies. It had been shown that the simulated disc galaxies have unrealistic rotation curves with sharp peaks at their centres declining at larger radii (Navarro & Benz 1991; Navarro & Steinmetz 1997; Weil et al. 1998; Abadi et al. 2003; Piontek & Steinmetz 2011; Hummels & Bryan 2012), which disagrees with the observations (Rubin et al. 1985). This is a result of the simulated galaxies having too little angular momentum because of their merging history which is inherent in the standard model by virtue of dynamical friction between the dark matter haloes, and because the gaseous baryons lose orbital energy by being compressed and by dissipating kinetic energy as they fall into the deep potential well of a dark matter halo.

Recent studies claim that disc galaxies with ‘realistic’ shapes of rotation curves can form in cosmological simulations with gas by using a subgrid model which enhances the efficiency of stellar feedback (Governato et al. 2010; Agertz et al. 2011; Guedes et al. 2011; Stinson et al. 2013; Aumer et al. 2013; Marinacci et al. 2013). Note that the feedback processes of model disc galaxies are fitted artificially to “agree with” the observations, and these feedback processes are neither natural results of the cosmological simulations nor predictions of dark matter. This also applies to the recent results from the Illustris project: the feedback applied there is unphysical and the BTFR comes out incorrectly (Vogelsberger et al. 2014; Kroupa 2014). Another criticism of the feedback processes can be found in the most re-

cent EAGLE project publication (Schaye et al. 2014). However, in spite of the artificiality of feedback processes, we would like to know: how realistic are these model disc galaxies?

If the simulated disc galaxies represent real galaxies, there should be a MDA correlation in these galaxies, and such relations have to agree with the empirical data. We here study the MDA correlation of simulated disc galaxies (Agertz et al. 2011; Guedes et al. 2011; Aumer et al. 2013; Marinacci et al. 2013), which are claimed to be more realistic than obtained in previous work and which are taken to demonstrate that the standard cosmological model can, after all, account for the observed galaxies.

Apart from the problems of rotation curves, there are other difficulties with the Λ CDM cosmology simulations on galactic scales, such as the cusp vs core problem (Springel et al. 2008) and the missing satellites problem (or more correctly, the satellite over-prediction problem) (Klypin et al. 1999; Moore et al. 1999) and many other failures to account for data (Kroupa et al. 2010; Kroupa 2012; Famaey & McGaugh 2012; Kroupa 2014). To overcome these difficulties, an alternative dark matter particle has been proposed, a thermal relic WDM particle with a keV mass scale (Colín et al. 2000; Bode et al. 2001; Gao & Theuns 2007; Schneider et al. 2012). The time scale for structure formation in the WDM cosmology is longer than that in the CDM cosmology, and the amount of sub-structures is decreased. The pioneering work on the formation of disc galaxies in WDM cosmological models is carried out by Herpich et al. (2013), according to which the disc galaxies have less centrally concentrated stellar profiles in improved agreement with real galaxies.

We here also study the MDA correlation of these galaxies. The circular velocities of galaxies contributed from baryons, v_b , and from dark matter, v_{DM} , are taken from the above simulations. The mass discrepancy is

$$\left[\frac{v(r)}{v_b(r)} \right]^2 = \frac{v_b^2(r) + v_{DM}^2(r)}{v_b^2(r)}. \quad (12)$$

The Newtonian acceleration (from baryons only) can be calculated from the circular velocity,

$$g_N(r) = v_b^2(r). \quad (13)$$

3.1 Disc galaxies from CDM cosmological simulations

In the dark-matter approach, there are two primary formation scenarios for disc galaxies. The first one was studied by Eggen et al. (1962); Samland & Gerhard (2003) and Sommer-Larsen et al. (2003, model S1), which is to form a disc galaxy in a growing dark matter halo by accreting gas (and also dark matter in Samland & Gerhard 2003) in the absence of mergers of dark haloes. This work was generally not accepted by the community because it lacked a “realistic” merging history. The second scenario is to form disc galaxies through accreting a large number of satellite galaxies (so called minor mergers, e.g., Bullock & Johnston 2005; Moore et al. 2006). The latter scenario was more favoured since it is consistent with the hierarchical assembly of CDM haloes in cosmological simulations (Helmi 2008). However,

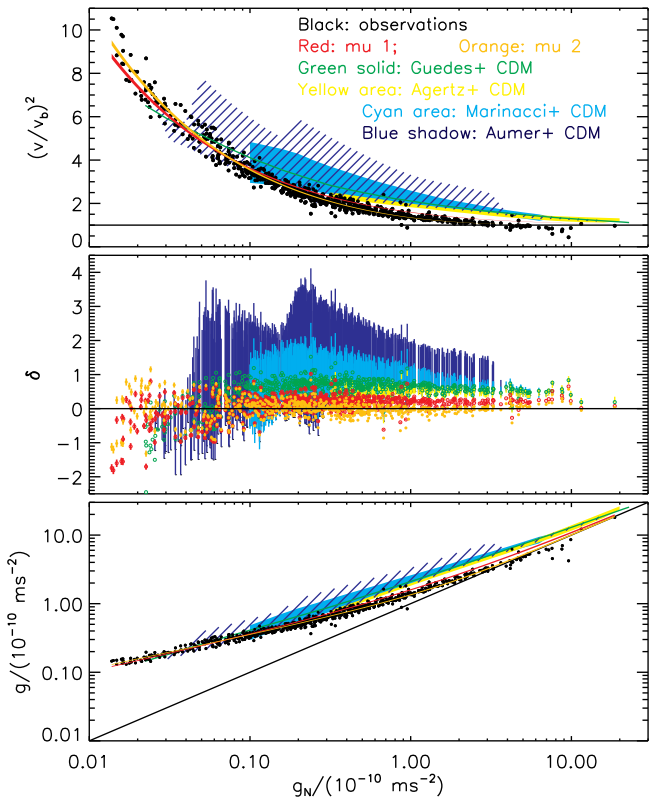


Figure 2. Upper panel: the mass discrepancy $(v/v_b)^2$ versus baryonic acceleration, g_N , from weak to strong fields. The black points are the observed MDA data by McGaugh (2004) for a sample of 74 disc galaxies, including both dwarf and Milky Way-scale spiral galaxies. The red and orange areas are the correlations predicted by Milgromian dynamics with different interpolating functions, red for simple μ and orange for standard μ (Eq. 10). The values of a_0 and the corresponding error are listed in the 6_{th} and 7_{th} columns of Table 1. The green curve shows the mass discrepancy-acceleration relation of simulated Milky Way-scale galaxies by Guedes et al. (2011). The coloured shadow areas are the mass discrepancy-baryonic gravitational acceleration data for simulated galaxies from cold dark matter cosmological simulations (upper panel Agertz et al. 2011; Marinacci et al. 2013; Aumer et al. 2013). Middle panel: the difference of the mass discrepancy between CDM models and observed galaxies, δ , which is defined in Eq. 14. For the simulated and observed galaxies g_N is computed from Eq. 13. Note that Milgromian dynamics with the standard μ function (orange curve) is an excellent description of the data (black dots in upper panel), the differences of which to the Milgromian dynamics relation are plotted as orange dots. The red dots are the differences between the observed (black points) and the Milgromian dynamics curve with the simple μ function. The apparent larger scatter in the orange δ values at small g_N is expected for a constant (small) dispersion of data around the Milgromian dynamics curve. Lower panel: the kinematic-luminous acceleration relation of the CDM models and the observed galaxies (symbols and colors as in the upper panel). The black line corresponds to $g = g_N$.

it is difficult to produce disc-dominated and bulgeless galaxies from the simulations of cosmological mergers, while there is a large fraction ($\approx 70\%$) of edge-on disc galaxies which are bulgeless or disc-dominated in observations (in a complete and homogeneous sample of 15127 edge-on disc galaxies in the SDSS data release 6, Kautsch 2009). HST photometry and Hobby-Eberly Telescope (HET) spectroscopy of giant Sc-Scd galaxies (Kormendy et al. 2010) also shows that more than 50% of a sample of 19 galaxies are bulgeless galaxies, which challenges the picture of galaxy formation by hierarchical merging. Baryonic feedback processes have been studied so as to save the second scenario (e.g., Okamoto et al. 2005; Piontek & Steinmetz 2011; Scannapieco et al. 2012). However it has been shown that the angular momentum problem of the simulated disc-dominated galaxies and bulgeless galaxies cannot be solved by adding feedback process and by increasing the numerical resolution of the simulations (e.g. D’Onghia & Burkert 2004; Piontek & Steinmetz 2011).

In a more recent study based on the Millennium-II simulations (Fakhouri et al. 2010) about 31% of the Galaxy-scale haloes have experienced a major merger since $z = 1$ (corresponding to a look-back time of about 7 – 8 Gyr), and the fraction of major mergers rises to 69% since $z = 3$ (corresponding to a look-back time of about 11 – 12 Gyr). Moreover, in cosmological simulations, over the last 10 Gyr for Galaxy-scale haloes with a mass of $\approx 10^{12} M_{\odot} h^{-1}$, 95% of them have undergone a minor merger by accreting a subhalo with mass $> 5 \times 10^{10} M_{\odot} h^{-1}$, and 70% of them have accreted a subhalo with mass $> 10^{11} M_{\odot} h^{-1}$ (Stewart et al. 2008). Therefore mergers are very common for Milky-Way-scale haloes in cosmological simulations. The simulations of major mergers (with equal mass galaxy pairs) show that the disc can be completely disrupted and that the remnants of such mergers become early-type galaxies (elliptical galaxies or bulge-dominated galaxies, Toomre 1977; Cox & Loeb 2008), and minor mergers (with a mass ratio 10 : 1) also lead to growth of the bulge and thickness of the disc (e.g., Walker et al. 1996; Naab & Burkert 2003; Younger et al. 2007; Kazantzidis et al. 2009). Thus, the very large fraction of observed bulgeless disc galaxies (70% in edge-on disc galaxies) is inconsistent with the high incidence ($> 70\%$) of significant mergers, a point also emphasized by Kormendy et al. (2010).

More recently, a series of new models using smoothed-particle hydrodynamics (SPH) simulations (Agertz et al. 2011; Guedes et al. 2011; Aumer et al. 2013; Marinacci et al. 2013) claimed that more realistic disc galaxies are formed in a quiet merger history scenario. In such a scenario no mergers with a mass ratio of the substructure and host galaxy larger than 1 : 10 are allowed at low redshift. These authors have thus, essentially, returned to the previously discussed models by Samland & Gerhard (2003) which, however, had been criticized as lacking cosmological realism by being void of mergers. Thus these galaxies are selected from the unlikely fraction of Milky-Way-scale haloes in standard cosmological simulations. It has been claimed that the rotation curves of these simulated galaxies have more reasonable shapes without sharp central peaks. To test these simulated galaxies more quantitatively and in more detail, we now study their MDA correlation, and then

compare the theoretical relation with that extracted from the observed galaxies.

The relation is shown in the upper panel of Fig. 2, where the green line, coloured shadows and areas represent the relations of disc galaxies in the aforementioned simulations, respectively. A correlation between the mass discrepancy at radius r , $\left[\frac{v(r)}{v_b(r)} \right]^2$, and the baryonic Newtonian acceleration at the same radius, Eq. 13, does exist in the simulated galaxies. However, despite the existence of such a correlation, the simulated galaxies are not consistent with observations. The MDA correlation obtained from the simulated disc galaxies (Agertz et al. 2011; Guedes et al. 2011; Aumer et al. 2013; Marinacci et al. 2013) lies significantly above the empirical relation. Among the above simulations, there is one Milky Way like disc galaxy modeled by Guedes et al. (2011), in which the trend of the mass discrepancy-acceleration relation is different from that obtained from the observed data points: with decrease of the acceleration, the increase of mass discrepancy is slower in the Guedes et al. (2011) model galaxy. Note that the disc galaxies in Agertz et al. (2011); Marinacci et al. (2013) and Guedes et al. (2011) are obtained from re-simulations of haloes with a quiet merger history, i.e., from haloes without major mergers at low redshift. The disc galaxies in Aumer et al. (2013) are selected from haloes both with and without low-z major mergers. There is a much wider spread and a larger deviation from the observational data for these Aumer et al. (2013) galaxies compared to other samples, and this could be an effect of the low-z mergers.

Although there is an overlap of the MDA correlations from simulations and observations in the weak field regime where $g_N < 0.1a_0$, the majority of MDA correlations predicted from the re-simulated disc galaxies are inconsistent with observations. More concretely, for a given enclosed baryonic mass M_b , the mass discrepancy is always overpredicted.

Therefore, considering the detailed rotation curves of galaxies simulated in a CDM universe, the simulated galaxies do not agree with the observed ones. The host dark matter haloes have to bear very quiet merger histories. Since the vast majority of local galaxies (72% spiral galaxies and 15% S0 galaxies, overall 87%) are disc galaxies (Delgado-Serrano et al. 2010), this generates another severe issue that cannot be resolved within the dark matter models.

The middle panel of Fig. 2 shows the difference of the MDA correlation between the simulated $\left[\frac{v(g_N)}{v_b(g_N)} \right]_{\text{CDM}}^2$ and the observed galaxies $\left[\frac{v(g_N)}{v_b(g_N)} \right]_{\text{obs}}^2$, δ (Eq. 14 below). Here the values of g_N for the observed galaxies are computed from Eq. 13. For most of the data points of the simulated galaxies, the mass discrepancy is always larger than for the observed galaxies. On the other hand, the observed data agree extremely well with Milgromian dynamics (i.e., with there being no cold or warm dark matter) with a standard μ -function (orange areas and symbols with error bars in Fig. 2) and with a simple μ -function (red areas and symbols with error bars in Fig. 2). The best fitting values of a_0 and the corresponding errors with different μ functions are computed with the Levenberg-Marquardt method, and are listed in the 6_{th} and 7_{th} columns of Table 1. With a simple μ -function (red areas and symbols in Fig. 2), the predictions of

mass discrepancy in Milgromian dynamics are slightly larger than the observations. Therefore, the standard μ -function is a better interpolating function for the MDA correlations.

We also notice that the dispersion of the relation for the simulated galaxies in the Λ CDM model is much wider than that of the observational data, especially in the weak acceleration regime. However, the correlation is tight for the observed galaxies. This is surprising because the observational points have measurement uncertainties which enlarge any spread. The wide spread of the theoretical relation comes about because the spatial distribution of dark matter does not tightly correlate with the baryonic distribution in different simulated galaxies. Such a wide spread is due to the multiplicity of free parameters of dark haloes: the parameters of the dark matter profiles are not unique for different modeled disc galaxies, the shapes of the dark haloes are tri-axial, and there is a variation between the inclination angle for the principle axes of the dark haloes and the baryonic discs (as emphasized by Disney et al. 2008). Instead, the observational data demonstrate a very close one-to-one relationship between the baryons and their rotation about the centre of their galaxy.

The lower panel of Fig. 2 shows the kinematic-luminous acceleration relation of the simulated galaxies from Λ CDM cosmological simulations (the coloured areas and shadows) and of the observed galaxies (black points). The predictions from Milgromian dynamic with two μ -functions are plotted (red area for the simple μ -function and orange area for the standard μ -function) as well. The kinematic-luminous acceleration relation of the simulated galaxies lies above that of the observed galaxies, and there is a much wider spread of such a relation for the simulated galaxies. This is not surprising, since the kinematic-luminous acceleration relation is exactly the MDA correlation plotted differently and the MDA correlation already indicates the disagreement between the simulated and the observed galaxies. Due to the stochastic galaxy formation scenario in cosmological simulations (Boylan-Kolchin et al. 2011), for a given enclosed baryonic mass, there are various possibilities for the centrifugal acceleration of the simulated galaxies. Therefore a tight correlation is not expected from the model galaxies. For a comparison, Milgromian dynamics predicts tight relations (with different forms of the μ -functions) for the MDA.

In summary, there are two problems for galaxy formation in Λ CDM cosmology: (i) the fraction of CDM haloes with a sufficiently quiet merging history is far too small to account for the large fraction of galaxies that are bulgeless discs or disc-dominated galaxies. (ii) Even those delicately selected DM haloes that do have a quiet merging history fail to host disc galaxies which correspond to real observed galaxies. Only the slow growth of the baryonic disc with the DM halo without any mergers has yielded realistic-looking disc galaxies, as already shown by Samland & Gerhard (2003). This is, however, equivalent to a growing purely baryonic galaxy in Milgromian dynamics.

3.2 Disc galaxies from WDM cosmological simulations

Herpich et al. (2013) simulated three galaxies, and the circular velocities contributed from baryons and dark matter can be found for two galaxies from the three (fig. 3 of Herpich

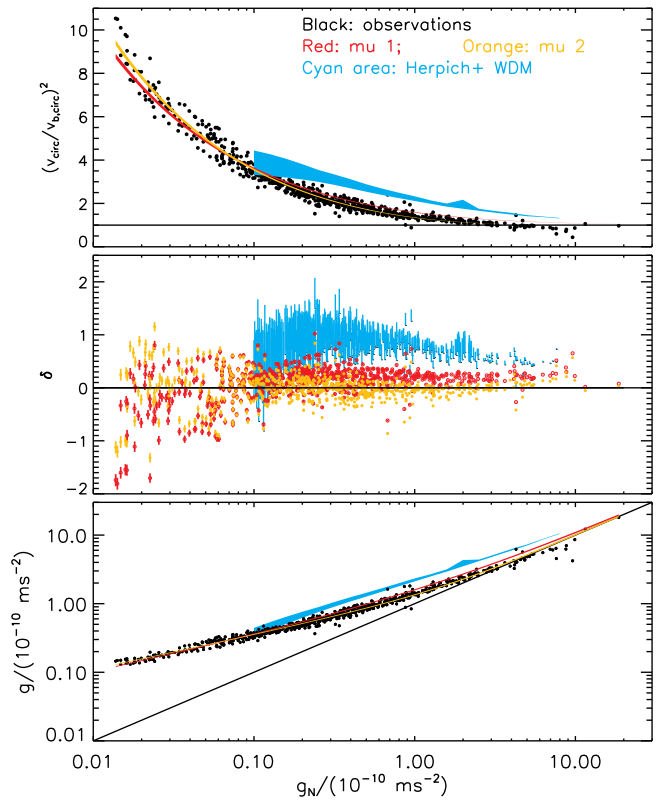


Figure 3. Upper panel: The black points and coloured areas are defined as in Fig. 2. The cyan areas are the mass discrepancy-baryonic gravitational acceleration relation for simulated galaxies from warm dark matter (Herpich et al. 2013) cosmological simulations. Middle panel: the difference of the mass discrepancy between WDM models and observed galaxies, δ (Eq. 14 below). Lower panel: the kinematic-luminous acceleration relation of the CDM models and the observed galaxies (symbols and colours as in the upper panel).

et al. 2013), g1536 and g5664, which are used here. For each galaxy, there are three sets of parameters, corresponding to different masses of the WDM particles. The MDA correlation for galaxies simulated in a WDM cosmology is presented in the upper panel of Fig. 3 with the cyan area. The difference of the MDA data between the WDM simulated galaxies $\left[\frac{v(g_N)}{v_b(g_N)} \right]_{\text{WDM}}^2$ and the observations $\left[\frac{v(g_N)}{v_b(g_N)} \right]_{\text{obs}}^2$, δ , is given by Eq. 14 below and is shown in the middle panel. The kinematic-luminous-acceleration relation for the WDM simulated galaxies is shown in the lower panel of Fig. 3. The MDA correlation is not consistent with the observations. The relations obtained from the simulated galaxies lie above the observational relation. Therefore, the above MDA data rule out the two model galaxies obtained from WDM simulations as well.

In Fig. 3, a comparison of the observational MDA data predicted under the assumption of Milgromian dynamics with a standard μ -function (orange areas and symbols) and a simple μ -function (red areas and symbols) is shown. It confirms again that the dispersion of the MDA data predicted by WDM models is larger than for Milgromian dynamics

with a standard μ -function and a simple μ -function. This is a result of the spread of WDM halo properties for a given baryonic mass (compare with Disney et al. 2008).

3.3 The Wilcoxon signed-rank test

As mentioned above (Sec. 3.1 and Sec. 3.2), the majority of the MDA data obtained from the C/WDM simulated galaxies lie above the relation obtained from the observations. Here we apply a non-parametric statistical hypothesis test, the Wilcoxon signed-rank test (Wilcoxon 1945; Bhattacharyya & Johnson 1977), to formally study the difference of the data between the simulations and the observations. The procedure of the Wilcoxon signed-rank test applied here is as follows:

- 1. For the observed data (i.e., McGaugh 2004 data) there are m data points. For each data point the values of g_N (defined in Eq. 13) and the ratio $\left[\frac{v(g_N)}{v_b(g_N)} \right]^2$ (data from McGaugh 2004) are known. To compare the observed data with the simulated galaxies, interpolate the upper envelope of the MDA data of the simulated galaxies at each observed data point $g_{N,i}$, where $i = 1, \dots, m$. Compute the difference of the MDA correlation between the simulated and the observed galaxies at each $g_{N,i}$, which is defined in Eq. 13,

$$\delta_i = \left[\frac{v(g_{N,i})}{v_b(g_{N,i})} \right]_{\text{C/WDM}}^2 - \left[\frac{v(g_{N,i})}{v_b(g_{N,i})} \right]_{\text{obs}}^2. \quad (14)$$

- 2. Exclude the simulated-observed data pairs with $|\delta_i| = 0.0$.³ Order the remaining data pairs according to increasing $|\delta_i|$. The number of the remaining data pairs is n . The rank of the data pairs is denoted as R_i .

- 3. The data pairs with $\delta_i > 0$ are selected, and the sum of their ranks are denoted as T^+ . Let

$$E = \frac{n(n+1)}{4}, \quad (15)$$

$$D = \frac{n(n+1)(n+2)}{24}. \quad (16)$$

There could be a group of ties within which the $|\delta|$ values of the elements are the same, i.e., $|\delta_i| = |\delta_a| = |\delta_b| = \dots$ ($i \neq a \neq b \neq \dots$). Let

$$Q = \frac{1}{48} \sum_{j=1}^l q_j (q_j^2 - 1), \quad (17)$$

where l is the number of such ties, and q_j is the number of elements in the j_{th} tie.

- 4. Calculate the statistic Z for a large sample of data pairs (for more details of the statistical method, see Bhattacharyya & Johnson 1977, p. 519),

$$Z = \frac{T^+ - E}{\sqrt{D - Q}}. \quad (18)$$

³ This is the standard procedure of the Wilcoxon sign rank test. However, in the data sample used here, there is no data pair with $|\delta_i| = 0.0$. The number of remaining data pairs is thus m .

- 5. Interpolate the lower envelope of the MDA data of the simulated galaxies at each $g_{N,i}$, and repeat the steps 1 – 4.

To test how well the MDA correlation predicted by Milgromian dynamics matches the observations, steps 1 – 4 are repeated for Milgromian dynamics with different μ functions. For each μ function, a Levenberg-Marquardt fit to the observed MDA data is applied to obtain the best fitting values of a_0 and the corresponding errors. The results are listed in Table 1. All of the CDM and WDM models, together with Milgromian dynamics with the simple μ -function, can be ruled out with a confidence of better than 99.99%. Only under Milgromian dynamics with the standard μ -function, $Z = 0.71$. Since the level of significance for exclusion and for a directional (1-tailed) test is $\alpha = 0.05$ for $Z = 1.645$, Milgromian dynamics with the standard μ -function constitutes a good description of the observed data. That is, the hypothesis that Milgromian dynamics/MOND does not agree with the MDA data can be ruled out with at most $1 - 2\alpha = 90\%$ confidence.

Finally, we test the MDA correlation in the pure SID regime (Sec. 2). Steps 1 – 4 are repeated for the data pairs with weak accelerations, $g_N < 0.2 \times 10^{-10} \text{ m s}^{-2}$, and the best fitting value of $a_0 = 1.24 \times 10^{-10} \text{ m s}^{-2}$ (Tab. 1). $Z = -0.38$ is obtained. This is an extremely good agreement between SID and the observed data. The level of significance for a 1-tailed standard normal critical value is -1.282 corresponding to $\alpha = 0.1$. Thus the hypothesis that SID does not agree with the MDA data in the weak field regime can be rejected with at most $1 - 2\alpha = 80\%$ confidence.

4 THE DARK MATTER HALO TO STELLAR MASS RELATION

4.1 The masses of CDM haloes

Above we have seen that the most advanced models based on Einsteinian/Newtonian gravitation together with cold or warm dark matter (DM) are not able to reproduce the observed MDA correlation. Another related way to test for the existence of dark matter haloes is to study the dark-matter-halo-mass versus baryonic-mass correlation. Recently, Miller et al. (2014) constrained the stellar to halo mass relation for a sample of 41 dwarf galaxies within a redshift range of $0 < z < 1$ (the positions, stellar and dark halo masses of the galaxies are listed in Tab. 2): the stellar masses, M_s , are derived from the Fitting and Assessment of Synthetic Templates (Kriek et al. 2009) code for the photometric database (Newman et al. 2013), and the DM halo masses, M_{vir} , are computed from

$$\log_{10}(M_{\text{vir}}/h^{-1}) = 3 \log_{10}(G^{-1}V_{200}) \quad (19)$$

assuming the haloes are spherical. Here $h = H_0/100 \text{ km s}^{-1} \text{ Mpc}^{-1}$, V_{200} is the rotation speed at the virial radius, r_{vir} , within which the enclosed CDM halo mass has a mean overdensity of 200 times of the critical density of the Universe, $\rho_{\text{crit}} = \frac{3H_0^2}{8\pi G}$. The parameters of their cosmological model are $\Omega_\Lambda = 0.7$, $\Omega_m = 0.3$, $H_0 = 70 \text{ km s}^{-1} \text{ Mpc}^{-1}$. V_{200} is converted according to

Table 1. Wilcoxon signed-rank test. The size of the sample of non-zero-differences of simulated-observed data pairs is $n = 730$. The first column tabulates the data source from the simulated galaxies, the 2_{nd} and 4_{th} columns contain the number of data pairs with $|\delta| > 0.0$ for the lower and upper envelopes of the simulated galaxies, respectively. The 3_{rd} and 5_{th} columns list, respectively, the statistic Z for the lower and upper envelopes of the simulated galaxies. The 6_{th} column lists the values of a_0 for different μ functions. For Guedes+’s model, there is only one simulated galaxy (no lower envelope). The results assuming SID and the transition regime are valid, with the simple and standard μ -functions, are listed in the 8_{th} and 9_{th} lines, respectively. The bottom line show the Wilcoxon signed-rank test for pure SID in the weak field regime (i.e., without the μ function), where $g_N < 0.2 \times 10^{-10} \text{ m s}^{-2}$. n^- is the number of the data pairs with $|\delta| < 0.0$.

DM simulated galaxies	Lower n^+	envelopes Z	Upper n^+	envelopes Z	best-fit a_0 $10^{-10} \text{ m s}^{-2}$
Marinacci+	467	24.84	539	28.41	
Agertz+	278	20.41	286	20.70	
Aumer+	424	10.53	681	32.05	
Guedes+	-	-	654	29.01	
Herpich+ (WDM)	527	28.27	536	28.33	
MOND simple μ	-	-	574	18.86	0.94 ± 0.03
MOND standard μ	-	-	375	0.71	1.21 ± 0.03
deep MOND ($g_N < 0.2 \times 10^{-10} \text{ m s}^{-2}$)	n^- 289	n^- 154	n^+ 135	Z -0.38	a_0 1.24 ± 0.03

$$V_{2.2}/V_{200} = 1.05, \quad (20)$$

where $V_{2.2}$ is a direct measurement of the circular velocity at the radius $r_{2.2}$ which is 2.2 times the scale radius (for more details, see Sec. 3.3 and Sec.4 in Miller et al. 2014). Note that this is an empirical relation measured from weak lensing by Reyes et al. (2012) for galaxies within the mass range of $[10^9, 10^{11}] \text{ M}_\odot$, and the slope of velocity ratio to stellar masses is 0.53 ± 0.03 . Miller et al. (2014) extrapolated this relation to low mass dwarf galaxies with masses of 10^7 M_\odot , thus the dispersion of V_{200} of the haloes derived from this relation is largest for the low-mass galaxies (see figures 6-7 in Miller et al. 2014). Since the ‘virial mass’ in Miller et al. (2014) is not derived from dynamics, it does not exactly amount to the virial mass defined in Eq. 21 and Eq. 22 below.

Miller et al. (2014) compared their observations with CDM cosmological simulations by Behroozi et al. (2013) within a similar redshift range. They found that the stellar to halo mass relation predicted from the simulated dwarf galaxies is at odds with observations. For a given stellar mass, the simulations significantly over-predict the mass of dark matter for the dwarf galaxies. Although the dispersion of data for the dwarf galaxies is large, the trend is clear that the observed data are not consistent with the curves from the simulated galaxies. This problem is essentially the same as that of the MDA correlation at large galactic radii, i.e., at low acceleration (see Fig. 2-3).

Furthermore, Guo et al. (2010) proposed an abundance-matching stellar to halo mass relation for model galaxies from Λ CDM cosmological simulations. However, in the low stellar mass range $[10^6, 10^8] \text{ M}_\odot$, the theoretical halo masses are too large by a factor of 5 compared to those of dwarf galaxies in a large survey of SDSS central galaxies⁴ (More et al. 2009). Ferrero et al.

(2012) improved the Guo et al. (2010) stellar to halo mass relation as follows:

$$\frac{M_s}{M_{\text{vir}}} = c \left[1 + \left(\frac{M_{\text{vir}}}{M_1} \right)^{-2} \right]^\kappa \left[\left(\frac{M_{\text{vir}}}{M_0} \right)^{-\alpha} + \left(\frac{M_{\text{vir}}}{M_0} \right)^\beta \right]^{-\gamma}, \quad (21)$$

where $c = 0.129$, $M_0 = 10^{11.4} \text{ M}_\odot$, $M_1 = 10^{10.65} \text{ M}_\odot$, $\alpha = 0.926$, $\beta = 0.261$ and $\gamma = 2.440$. κ is a free parameter. Larger values of κ represent shallower stellar to halo mass relations for low mass haloes, while $\kappa = 0$ returns to the abundance-matching relation proposed by Guo et al. (2010). We note that the procedure to associate visible galaxies with their dark matter haloes which are derived from dark-matter-only simulations lacks the physics of galaxy formation entirely. Abundance-matching is merely the short-circuiting of a major problem of Λ CDM cosmology (the ‘missing dwarf galaxy problem’, or more truthfully ‘the dwarf over-prediction problem’).

We compare the halo to stellar masses predicted by Eq. 21 (cyan curves) for different values of κ to the empirical data of Miller et al. (2014) in Fig. 4, finding an inconsistency between the simulated and observed galaxies. For a given stellar mass, the halo mass is significantly over-predicted for Ferrero’s relation for all different values of κ .

4.2 The mass of the phantom dark matter halo

Concerning Milgromian dynamics, a baryonic object is surrounded by an unreal non-particle (i.e., phantom) isothermal dark matter halo with constant circular velocity given by Eq. 6. This follows directly from pure-SID, i.e. even without considering the transition from pure-SID to the Newtonian regime, the description of which constitutes Milgromian dynamics (Appendix A) in the classical dynamical regime. The apparent phantom virial dark matter mass, M_{vir} , can

⁴ In Guo et al. (2010), the CDM (sub-)haloes are selected from all (sub-)haloes that have galaxies at their centres.

Table 2. The right ascensions and declinations (epoch J2000, the 2_{nd} and 3_{rd} columns), stellar masses (the 4_{th} column) and halo masses (the 5_{th} column) of dwarf galaxies in Miller et al. (2014). The strength of the external field (Eq. 30) is listed in the 6_{th} column for the labeled magenta dwarf galaxies in Fig. 4, assuming $M_b = M_s$. Here $a_0 = 1.21 \times 10^{-10} \text{ m s}^{-2}$ as in Tab. 1.

Number	R.A.	Dec.	Log(M_s/M_\odot)	Log(M_{vir}/M_\odot)	g_e/a_0
1	34.287564	-5.1435433	8.74 \pm 0.09	10.79 \pm 0.03	
2	34.303787	-5.1458641	8.32 \pm 0.12	10.39 \pm 0.15	
3	34.358524	-5.1515666	7.84 \pm 0.09	9.36 \pm 0.39	
4	34.398975	-5.1525832	8.79 \pm 0.07	10.70 \pm 0.14	
5	34.289186	-5.1563347	8.31 \pm 0.09	9.80 \pm 0.35	
6	34.359126	-5.1571952	7.29 \pm 0.14	9.68 \pm 0.30	
7	34.336092	-5.1585409	7.83 \pm 0.08	9.56 \pm 0.13	0.019
8	34.489719	-5.1596155	8.64 \pm 0.14	10.78 \pm 0.32	
9	34.404135	-5.1638168	8.43 \pm 0.06	10.20 \pm 0.09	
10	34.310380	-5.1642154	8.54 \pm 0.13	10.44 \pm 0.20	
11	34.367527	-5.1671357	8.41 \pm 0.08	10.47 \pm 0.27	
12	34.440428	-5.1676006	8.74 \pm 0.09	10.55 \pm 0.21	
13	34.473897	-5.1691046	7.76 \pm 0.11	9.71 \pm 0.25	
14	34.446086	-5.1700983	8.15 \pm 0.15	9.71 \pm 0.08	0.028
15	34.279085	-5.1710765	8.30 \pm 0.06	10.38 \pm 0.16	
16	34.350739	-5.1712933	7.25 \pm 0.11	9.26 \pm 0.18	
17	34.503690	-5.1738860	8.27 \pm 0.08	10.09 \pm 0.18	
18	34.432528	-5.1760097	8.75 \pm 0.09	10.64 \pm 0.06	
19	34.466202	-5.1780329	8.76 \pm 0.10	10.46 \pm 0.03	0.020
20	34.429762	-5.1785330	8.96 \pm 0.06	11.09 \pm 0.17	
21	34.434409	-5.1793119	8.50 \pm 0.08	10.46 \pm 0.40	
22	34.517196	-5.1793529	7.89 \pm 0.07	9.68 \pm 0.20	
23	34.250846	-5.1797838	7.60 \pm 0.13	9.92 \pm 0.09	
24	34.415249	-5.1820298	8.50 \pm 0.08	10.39 \pm 0.06	
25	34.296140	-5.1827143	8.13 \pm 0.12	9.94 \pm 0.06	0.015
26	34.362769	-5.1829861	8.03 \pm 0.09	9.67 \pm 0.08	0.023
27	34.477748	-5.1834746	7.46 \pm 0.11	9.75 \pm 0.03	
28	34.423177	-5.1861241	7.95 \pm 0.08	9.92 \pm 0.23	
29	34.282862	-5.1864030	8.02 \pm 0.07	10.11 \pm 0.15	
30	34.520764	-5.1871599	7.06 \pm 0.27	9.31 \pm 0.31	
31	34.413980	-5.1882020	8.20 \pm 0.20	9.96 \pm 0.09	0.017
32	34.523446	-5.1899136	7.40 \pm 0.21	9.62 \pm 0.21	
33	34.254774	-5.1914894	8.50 \pm 0.08	10.45 \pm 0.19	
34	34.359852	-5.1916576	8.66 \pm 0.14	10.30 \pm 0.35	
35	34.417074	-5.1950333	8.36 \pm 0.11	9.95 \pm 0.13	0.026
36	34.370424	-5.2035566	8.80 \pm 0.11	10.67 \pm 0.02	0.013
37	34.465397	-5.2073517	8.82 \pm 0.07	10.64 \pm 0.13	
38	34.446346	-5.1498754	9.24 \pm 0.12	10.95 \pm 0.09	
39	34.283345	-5.1519078	9.06 \pm 0.13	10.96 \pm 0.08	
40	34.392003	-5.1590678	8.94 \pm 0.07	10.83 \pm 0.17	
41	34.275351	-5.1724717	9.08 \pm 0.16	10.96 \pm 0.05	

be derived from Eq. 6 (for the derivation, see Sec. 2.1 in Wu & Kroupa 2013), which is ⁵

⁵ The virial mass in SID can be derived in the same way as in Miller et al. (2014), i.e., from a relation between V_{200} and $V_{2.2}$ in SID. The derivation of such a “virial mass” is presented in Appendix B. However, because the errors of the Tully-Fisher (TF) relation in the galaxies of Miller et al. (2014) are large, and the fit parameters for the TF relation are significantly different for different samples of galaxies (see table 2 in Miller et al. 2014), the so-obtained “virial mass” is strongly sample dependent. Therefore a more universal virial mass of a galaxy in SID is adopted in Sec. 4.2. Essentially, we assume that the inner rotation velocity (see Sec. 4.1) is a measure of the flat part of the rotation velocity at larger radii, which in turn measures the mass of the dark matter halo.

$$M_{\text{vir}} = (G a_0 M_b)^{3/4} p^{-1/2} G^{-3/2}, \quad (22)$$

$$p = \frac{4}{3} \pi \times 200 \rho_{\text{crit.}}$$

Such phantom dark matter haloes are associated with a non-inertial (i.e., unreal) mass by a Newtonian observer. *That is, an observer interpreting the motion of a star around a galaxy in terms of Newtonian dynamics will deduce (wrongly) that the galaxy is immersed in a dark matter halo. However, the inertial mass of the galaxy is exactly its baryonic mass only.*

Therefore, the phantom dark matter halo mass is sourced entirely by the baryonic mass of the galaxy (Eq. 22). The phantom halo to baryonic (stellar plus gas) mass ratio follows from Eq. 22,

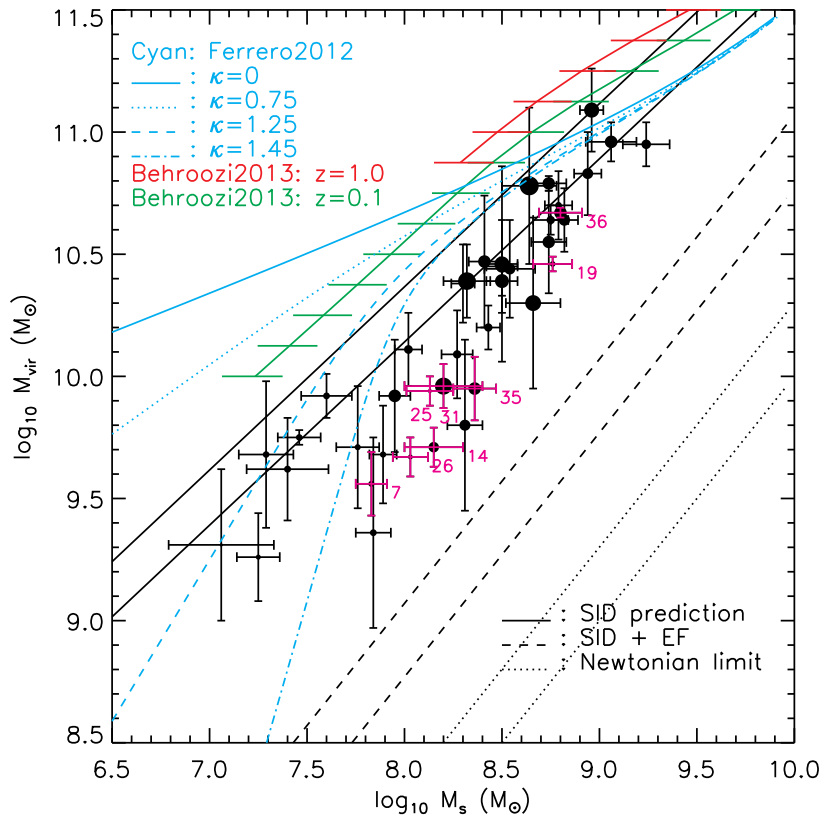


Figure 4. The halo to baryonic (stellar plus gas) mass relation from observations by Miller et al. (2014, black circles with error bars, the size of the symbols represents the redshift, $z \in (0, 1)$, of the dwarf galaxies: larger symbols for higher redshifts and smaller symbols for lower redshifts) and from simulated galaxies by Ferrero et al. (2012, cyan curves) and Behroozi et al. (2013, red and green curves, corresponding to $z = 1.0$ and 0.1 , respectively). The black lines are predictions from SID (Eq. 23): for isolated galaxies (solid lines, the upper is for assuming the mass of gaseous matter, M_g , equals to the mass of stars, M_s , in a galaxy and the lower solid line is for assuming the mass of gas $M_g = 0$ in a galaxy), for galaxies located at the position of the LMC near a Milky-Way-like galaxy (dashed lines, the upper and lower dashed lines are defined the same as solid lines) and for galaxies embedded in a strong external field (Newtonian limit, dotted lines, the upper and lower dashed lines are defined the same as solid lines). The magenta symbols point out the dwarf galaxies whose halo-to-baryonic mass ratio lies beyond the 3σ confidence level away from the prediction of SID, i.e., galaxies probably embedded in external fields. The magenta numbers show the numbers of the corresponding galaxies in Table 2.

$$\frac{M_{\text{vir}}}{M_b} = (G a_0)^{3/4} M_b^{-1/4} p^{-1/2} G^{-3/2}, \quad (23)$$

which is shown with two black solid lines in Fig. 4. Since the amount of gas is difficult to determine in the observations, the mass of gas is a parameter in SID/MOND which is not well constrained. Here $a_0 = 1.21 \times 10^{-10} \text{ m s}^{-2}$, which is the value determined by Begeman et al. (1991), and agrees with the best-fit value of the MDA data in Sec. 3.1. The upper limit for the mass of gas, M_g , is assumed to be the same as M_s , i.e., $M_b = 2M_s$. The lower limit for the mass of gas is $M_g = 0$, i.e., $M_b = M_s$. The two limits correspond to the upper and lower solid lines in Fig. 4. These two assumptions on the mass of gas most probably straddle the real gas content of the dwarf galaxies which is undetermined for the sample of Miller et al. (2014). The existence of gas decreases the halo to stellar mass ratio in Milgromian dynamics. There are overlaps between the prediction of Milgromian dynamics and CDM cosmological simulations for the isolated gas-

rich galaxies ($M_g = M_s$). However, the prediction based on Milgromian dynamics agrees much better with the observations within the error range of the data. The data which deviate more than 3σ from Eq. 23 are over-plotted using magenta symbols in Fig. 4. These data points are possibly the bad points of the sample, since the virial mass for the data points are obtained from the empirical relation of Eq. 20, and they are not exactly the virial mass derived from dark halo dynamics. Interestingly, SID predicts a truncated phantom halo which stays below the solid lines in the figure if its baryonic source system is exposed to an external field (see Sec. 4.3).

4.3 The external field effect in SID

4.3.1 The virial mass of a galaxy embedded in an external field

In SID/Milgromian dynamics there appears an interesting effect that leads to an observable prediction which does not

exist in the Newtonian plus dark matter model. It is relevant for a satellite object falling within the gravitational field of a host such that the host field does not vary significantly across the satellite. This external gravitational field effectively truncates the isothermal phantom dark matter halo, as deduced by an observer who interprets the observations within Newtonian dynamics. The Milgromian dynamics/MOND equation for a spherical, axisymmetric or cylindrical system embedded in an external field is (Milgrom 1983c; Sanders & McGaugh 2002)

$$\mathbf{g}_{N,i} + \mathbf{g}_{N,e} = \mu(|(\mathbf{g}_i + \mathbf{g}_e)|/a_0)(\mathbf{g}_i + \mathbf{g}_e), \quad (24)$$

where $\mathbf{g}_{N,i}$ is the Newtonian acceleration from the baryonic matter of the internal system, $\mathbf{g}_{N,e}$ is the Newtonian acceleration from the baryonic matter of the external gravitational source generating the background uniform field, and \mathbf{g}_i and \mathbf{g}_e are the internal and external gravitational accelerations. For an external field dominated system, $g_e = |\mathbf{g}_e| \gg g_i = |\mathbf{g}_i|$, Eq. 24 is expanded around g_e to lowest order as

$$\begin{aligned} g_{N,e} &= \mu(|\mathbf{g}_e|/a_0)\mathbf{g}_e, \\ g_{N,i} &= \mu(|\mathbf{g}_e|/a_0)\mathbf{g}_i, \end{aligned} \quad (25)$$

with a dilation factor of $\Delta_1 = (1 + d \ln \mu / d \ln x)_{x=g_e/a_0}$. Δ_1 approaches 1 in the Newtonian limit and approaches 2 in the deep MOND limit. The value of Δ_1 also depends on the direction relative to the external field (for more details see Milgrom 1983c; Bekenstein & Milgrom 1984; Zhao & Tian 2006). $\mu(x) = x$ in the low acceleration regime where SID is valid (i.e., in deep MOND limit).⁶

A star on a circular orbit at a large distance from the satellite galaxy with mass M_b orbits subject to the centrifugal acceleration $g_i = v^2/r$. In SID (Milgrom 2009c, 2014a) a Newtonian observer interprets this to be due to the centripetal acceleration from an isothermal (phantom) dark matter halo (PDMH) with mass within radius r of $M_{\text{PDMH}}(< r)$. Assuming spherical symmetry, it follows that

$$\frac{GM_{\text{PDMH}}(< r)}{r^2} = \frac{\sqrt{GM_b a_0}}{r}. \quad (26)$$

Thus, the mass of the phantom dark matter halo is

$$M_{\text{PDMH}}(< r) = (M_b a_0)^{1/2} G^{-1/2} r. \quad (27)$$

An isolated galaxy has an infinitely extended PDMH with an unbounded phantom mass. An isolated galaxy within

⁶ Note that SID as such does NOT necessary imply the introduction of a_0 , nor the role of acceleration. One can obtain SID by introducing a length scale factor, r_0 , instead of the introduction of a_0 , into the Newtonian law of gravity. Thus $g = GM/(r r_0)$ instead of the Newtonian spherical symmetric gravity, $g_N = GM/r^2$. One can also obtain SID by introducing a time constant, t_0 , such that the gravity becomes $g = (GM/t_0)^{2/3} r^{-1}$. Therefore SID is obtained from the above two examples, but the baryonic Tully-Fisher relations are different. $M \propto v^2$ for the length scale factor in the former case and $M \propto v^3$ for the time constant in the latter case, whereas $M \propto v^4$ through the introduction of a_0 in SID/MOND. Therefore, MOND is based on two main axioms: the introduction of a_0 as the role of an acceleration constant and SID is the deep MOND limit.

a cosmological model has a virial PDMH mass given by Eq. 22 above which follows from equating the mean PDMH density within r_{vir} to 200 times the critical density in the universe, yielding the maximum radius r_{vir} of the isothermal PDMH. If the galaxy is immersed in a uniform external gravitational field corresponding to an acceleration $\mathbf{g}_e = (0, 0, g_e)$ on a Cartesian grid, i.e., the external field is along the z -axis direction, then the centripetal acceleration from the PDMH, g_i , equals $g_e = |\mathbf{g}_e|$ at the radius $r_{\text{eq,SID}} = v^2/g_e = \sqrt{GM_b a_0}/g_e$. Using Eq. 27, the PDMH mass of such a galaxy is thus reduced in mass to the value

$$M_{\text{PDMH}}(r_{\text{eq,SID}}) = (M_b a_0)^{1/2} G^{-1/2} r_{\text{eq,SID}}. \quad (28)$$

At radius $r > r_{\text{eq,SID}}$ the star accelerates mainly according to \mathbf{g}_e , while at $r < r_{\text{eq,SID}}$ it accelerates mainly according to internal \mathbf{g}_i .

Thus, a strict prediction following from SID and thus from Milgromian dynamics (i.e. MOND) is that a Newtonian observer will deduce galaxies to have a maximal (phantom) dark matter halo mass given by $M_{\text{PDMH}} = M_{\text{vir}}$ (Eq. 22). Galaxies which are immersed in a uniform external field will appear to have reduced PDMH masses (Eq. 28). The two solid lines in Fig. 4 show the virial masses of isolated galaxies in SID. SID predicts that galaxies embedded in external fields stay below the solid lines in Fig. 4.

4.3.2 A distance—strength-of-external-field relation

At $r = r_{\text{eq,SID}}$, the strength of the external field as obtained by a Newtonian observer is

$$g_e = \frac{GM_{\text{PDMH}}(r_{\text{eq,SID}})}{r_{\text{eq,SID}}^2}. \quad (29)$$

For a given dwarf galaxy, the strength of the external field as a function of the observationally determined baryonic mass and the observationally determined phantom dark matter halo mass can be derived from the combination of $g_i(r_{\text{eq,SID}}) = g_e$, Eq. 6 and Eq. 29,

$$g_e = \frac{M_b}{M_{\text{PDMH}}} a_0, \quad (30)$$

where M_{PDMH} is the unreal phantom dark matter halo mass of the dwarf galaxy observationally deduced by a Newtonian observer. This simple relation supplies a quick way to determine the strength of an external field which a dwarf galaxy is exposed to if the baryonic and halo (or dynamical) mass of the galaxy are known.

For galaxies whose phantom halo masses deviate from the SID prediction (Eq. 23) by more than the 3σ confidence level (the magenta symbols and numbered labels in Fig. 4), the strength of their external fields (Eq. 30) are computed and listed in Table 2. The external fields are generally weak, from $0.01a_0$ to $0.03a_0$. In SID/Milgromian dynamics all the data points are expected to stay on (for the field galaxies) and below (for the dwarf galaxies near another gravitational source) the solid lines in Fig. 4: upper solid line for gas-rich galaxies and lower solid line for gas-poor galaxies.

Eq. 30 is a relation between the baryonic mass, $M_{b,\text{host}}$, of a nearby galaxy or cluster of galaxies generating the

required external field and the distance to the centre of the nearby gravitational source, d . For a given g_e , for example, as calculated from Eq. 30, $d = v_{\text{host}}^2/g_e$, where $v_{\text{host}} = (GM_{b,\text{host}}a_0)^{1/4}$, thus

$$d = \sqrt{GM_{b,\text{host}}a_0}/g_e. \quad (31)$$

Here v_{host} is the circular velocity of the host-galaxy's phantom dark matter halo generated by the host galaxy's baryonic mass, $M_{b,\text{host}}$. Fig. 5 shows the $d(M_{b,\text{host}})$ relation for the dwarf galaxies of Miller et al. (2014) assuming they are embedded in external fields, i.e., for the magenta symbols in Fig. 4, and assuming that for the dwarfs $M_b = M_s, M_g = 0$. If the nearby galaxy is also a dwarf galaxy, with a baryonic mass of $10^9 M_\odot$, the distances to the dwarf galaxies are only $40 - 90$ kpc, while if the nearby external field source is a rich cluster of galaxies with a baryonic mass of $10^{13} M_\odot$, the distances between the cluster centre and the Miller et al. (2013) dwarf galaxies are $4000 - 9000$ kpc.

For a comparison, we consider the Large Magellanic Cloud (LMC, dashed lines in Fig. 4, the upper line is for gas-rich galaxies, i.e., with the assumption of $M_b = 2M_s, M_g = M_s$, and the lower line is for gas-poor galaxies, i.e. with the assumption $M_b = M_s, M_g = 0$), which is located at a Galactocentric distance of 49.5 kpc (Kallivayalil et al. 2006). The LMC is embedded in the gravitational background field of the Milky Way (MW). To calculate the external field strength of the MW at the position of the LMC, the baryonic Milky Way model with an interpolating function of 'simple' μ form is used from Wu et al. (2008). For the MW as a host galaxy, $g_e \approx 0.17a_0$ for the LMC can be obtained from this model. All the 41 galaxies in Fig. 4 are above the halo to stellar mass relation of the LMC, since they are either isolated galaxies or embedded in external fields (see the 6_{th} column of Tab. 2) in general one order of magnitude smaller than that of the LMC. As a result, the phantom dark matter haloes have larger truncation radii, and the enclosed halo masses within the truncation radii are larger. The dashed line in Fig. 5 shows the $d(M_{b,\text{host}})$ relation for the external field of the LMC, and the circle represents the values of d and $M_{b,\text{host}}$ for the LMC in the Milky Way. For the dwarf galaxies of Miller et al. (2014) within an external field, i.e., the magenta symbols in Fig. 4, if the nearby galaxy is a Milky-Way like galaxy, the distances between the galaxy sourcing the external field and the dwarfs are about $200 - 400$ kpc (see Fig. 5).

SID/Milgromian dynamics predicts that for dwarf galaxies, the halo to baryonic mass relation has to stay in the range between the upper solid line (isolated galaxies) and the lower dashed line (galaxies embedded in an external field from a nearby massive galaxy) in Fig. 4. *Thus it is possible to falsify MOND by future observations of the stellar to halo mass relation of dwarf galaxies.* For example, an isolated field dwarf galaxy must appear near the solid lines of Fig. 4 since MOND would be falsified otherwise. Also, a self-gravitation satellite star cluster or dwarf galaxy will, as a result of the external field, compress as it orbits away from its host due to the build-up of its phantom dark matter halo, and conversely, it will expand on its orbit towards its host (Wu & Kroupa 2013). The same satellite will be larger in size near a more massive host. This may be the explanation

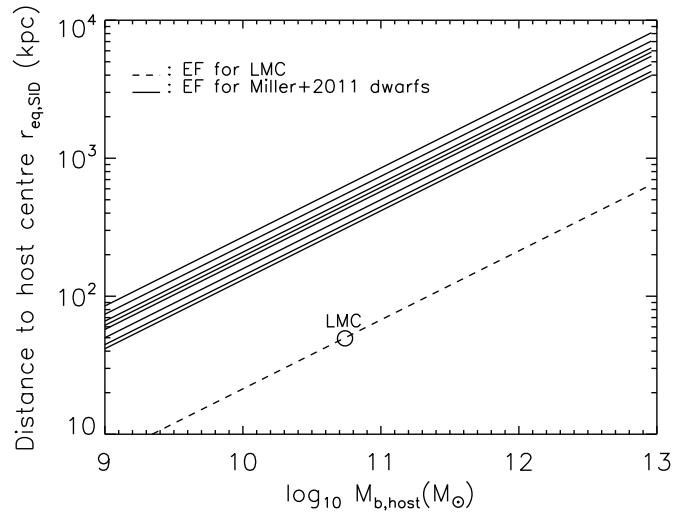


Figure 5. The $d(M_{b,\text{host}})$ relation (Eq. 31) for the dwarf galaxies of Miller et al. (2014) assuming they are embedded in an external field. Here d is the distance between a dwarf galaxy in the Miller et al. (2014) sample (labeled magenta in Fig. 4, from top to bottom are for models 36, 25, 31, 7, 18, 26, 35, 14 in Tab. 4) and the centre of the external field source (solid lines). $M_{b,\text{host}}$ is the baryonic mass of the external field source, which could be a nearby galaxy or a cluster of galaxies. The dashed line is the $d(M_{b,\text{host}})$ relation within an external field of $0.17a_0$, which is the strength of the external field at the LMC due to the Milky Way. The circle is the $(d, M_{b,\text{host}})$ position of the LMC.

why the Andromeda satellites have larger radii compared to the satellite galaxies of the Milky Way (Collins et al. 2011).

5 CONCLUSIONS

The observed centrifugal acceleration and the Newtonian acceleration for disc galaxies are extremely strongly correlated. In the weak field regime, where $g_N \ll a_0$, the correlation follows readily from SID (Sec. 2).

We showed that the mass discrepancy and the acceleration are correlated for disc galaxies simulated in CDM and WDM cosmological models. But, the correlation does not agree with the observations. This indicates that the best simulated disc galaxies, which are delicately chosen to have had a quiet merger history, even so still do not represent the correct rotation curves. In any case, the fraction of real galaxies without a bulge is far larger than the fraction of model galaxies in the dark matter framework which have no significant merger history, thus making the dark matter framework unlikely to work. The here reported analysis thus adds to the growing evidence that cold or warm dark matter does not exist. If so, then dynamical friction between galaxies on their dark matter halos would not be evident in the galaxy population as galaxies would merge rarely (Kroupa 2014). Recent additional evidence for a lack of mergers has been independently found by Lena et al. (2014).

Moreover, the dispersion of the MDA correlation in the weak acceleration regime that is obtained in the CDM and the WDM simulations is much wider than for the observational data. The tight correlation between the observed centrifugal acceleration and the Newtonian acceleration from

the observed baryon-only masses implies a small scatter of the baryonic Tully-Fisher relation (McGaugh 2004), which has been confirmed by the more recent observations of McGaugh (2012). On the other hand, the wide spread of the relation in CDM and WDM simulations indicates a large scatter of the baryonic Tully-Fisher relation, which is incompatible with the observations. The large scatter in the simulated Λ CDM and the WDM galaxies is a necessary feature of these models because the dark matter haloes have various shapes and masses for a given baryonic galaxy, as already noted by Disney et al. (2008). Instead, the Newtonian observer detects unphysical (i.e., phantom) dark matter halo masses which are due to Milgromian rather than Newtonian dynamics in the weak field regime.

The halo to baryonic mass relation is studied for cosmologically simulated galaxies and for SID. We find that SID (and thus MOND) predicts an apparent (phantom) virial halo to baryonic mass relation which agrees well with observations. The simulated galaxies from CDM models fail to reproduce the observed halo-to-stellar mass relation, thereby constituting another major problem of the particle dark matter models.

Finally, SID is studied for systems falling in an external field, assuming the field does not vary much across the system. This is the case when a star cluster or a satellite dwarf galaxy orbits within a much larger host field. The external field truncates the phantom dark matter halo radius, and therewith reduces the mass of the phantom dark matter halo. A $d(M_{b,\text{host}})$ relation is considered for the dwarf galaxies compiled by Miller et al. (2014) assuming they are embedded in an external field. SID predicts that for these galaxies there must be nearby gravitational sources like a companion galaxy or a cluster of galaxies. For each deviating dwarf galaxy, the distance to the external field source and the baryonic mass of the external field source follows a simple relation (Eq. 31), shown in Fig. 5. Also satellite galaxies near more massive hosts will have larger radii on average as a result of the truncation of their phantom dark matter halo masses due to the external field. The hitherto unexplained size difference between Andromeda and Milky Way satellites may be thus perhaps resolved. This implies that the gravitational forces acting between two galaxies vary with the position and mass of a third galaxy.

In summary, real galaxies follow SID/Milgromian dynamics rather than Newtonian dynamics, and reality is thus properly described by Milgromian dynamics (Famaey & McGaugh 2012; Kroupa 2012). Additional tests of Milgromian dynamics on star-cluster scales and on cosmological scales are required to further ascertain its range of validity.

6 ACKNOWLEDGMENTS

We thank Mordehai Milgrom for his helpful and important comments. We thank Stacy McGaugh for sharing his observational data of the mass discrepancy and acceleration of disc galaxies. Part of this work is done in Argelander-Institut für Astronomie der Universität Bonn, and Xufen Wu gratefully acknowledges support through the Alexander von Humboldt Foundation.

APPENDIX A: MILGROMIAN DYNAMICS/MOND

In this section a brief introduction to Milgromian dynamics (i.e. to Modified Newtonian Dynamics, MOND), is provided. The reader is referred to Famaey & McGaugh (2012) for a deep and thorough review of this topic. Essentially, MOND is the full classical description of gravitational dynamics encompassing the low-acceleration pure-SID (Sec. 2) regime and the Newtonian regime.

In addition to the major problems found in Λ cold dark matter (Λ CDM) cosmological simulations based on Newtonian/Einsteinian gravity (e.g. the cusp, the satellite over-prediction and the disc-of satellites problems, see Pawłowski et al. 2014; Ibata et al. 2014; Kroupa 2014, 2012; Springel et al. 2008; Klypin et al. 1999; Moore et al. 1999), it is also difficult to explain some puzzling conspiracies of C/WDM and baryons in galaxies by means of the current best AC/WDM models (Sanders 2009; Kroupa et al. 2010; Famaey & McGaugh 2012). For instance, there is an empirical relation between observed galaxy baryonic mass, i.e. the luminosity, and rotation speed. This is the baryonic Tully-Fisher relation (hereafter BTFR, Tully & Fisher 1977; McGaugh et al. 2000; McGaugh 2012), which cannot be naturally obtained in Λ CDM models (McGaugh 2012). Apart from the BTFR, there are other newly observed coincidences which are difficult to be reproduced in the simulated galaxies in the dark-matter framework, such as the observationally-deduced apparent dark matter content in the tidally formed dwarf galaxies (Gentile et al. 2007) and the discovery of a universal scale for the surface density of both the baryons and dark matter halo at the core radius of effective dark matter in a galaxy (Gentile et al. 2009; Milgrom 2009b). Indeed, the standard model of cosmology is in poor agreement with data and the hypothesis that C/WDM particles play a significant role in the universe has been seriously challenged if not ruled out (Sanders 2009; Kroupa et al. 2010; Kroupa 2012; Famaey & McGaugh 2012; Kroupa 2014).

Milgromian dynamics was originally proposed (Milgrom 1983c,a,b) to account for gravitational dynamics in the classical regime without introducing DM. With MOND, Milgrom extends our understanding of effective gravitational dynamics beyond the gravitational-dynamical systems known in 1916. Bekenstein & Milgrom (1984) demonstrated that MOND conserves momentum, energy and angular momentum in a self-gravitating system. In MOND the dynamical acceleration, $g = |\mathbf{g}| = \sqrt{g_N a_0}$, takes the place of Newtonian acceleration, g_N , in the weak field regime where $g \ll a_0$ and which is the regime of pure-SID (Sec. 2); while dynamical acceleration approaches Newtonian acceleration in the strong field regime, i.e., $g = g_N$ when $g \gg a_0$. The constant acceleration, $a_0 \simeq 1.21 \times 10^{-10} \text{ m s}^{-2} \approx 3.8 \text{ pc/Myr}^2$, is the critical value of acceleration which switches dynamics between Newtonian and Milgromian (e.g., Milgrom 1983c; Bekenstein & Milgrom 1984; Begeman et al. 1991; Kent 1987; Milgrom 1988; McGaugh 2011, 2012; Sanders & McGaugh 2002; Bekenstein 2006; Milgrom 2008). It is found to be in coincidence with various constants of cosmology, such as $a_0 \approx cH_0/2\pi$, $a_0 \approx c(\Lambda/3)^{1/2}/2\pi$, where c is the speed of light in vacuum, H_0 is the local Hubble constant and Λ is the cosmological constant (Milgrom 1983c, 1989, 2009c, 2014b).

MOND has until now passed all tests over a wide range of scales in different types of galaxies and naturally accounts for the aforementioned observations (Milgrom 1983c; Bekenstein & Milgrom 1984; McGaugh 2011, 2012; Milgrom & Sanders 2003; Sanders & Noordermeer 2007; Gentile et al. 2007, 2009; McGaugh 2004; Milgrom 2009b), such as the BTFR and the apparent dark matter content in tidal dwarf galaxies. Moreover, MOND is very successful in explaining the vertical kinematics of stars in galactic discs in the absence of dark matter (Bienaymé et al. 2009) and naturally accounts for the faster rotational speeds of polar rings (Lüghausen et al. 2013). Furthermore, there are other new covariant theories equivalent to MOND at their non-relativistic limit (Bekenstein 2004; Zlosnik et al. 2007; Bruneton & Esposito-Farèse 2007; Zhao 2007; Sanders 2005; Skordis 2008; Skordis & Zlosnik 2012; Halle et al. 2008; Milgrom 2009a).

APPENDIX B: VIRIAL MASSES CALCULATED BASED ON MILLER’S EMPIRICAL RELATION

The virial masses of particle dark matter halo masses cannot be measured directly. However, because the rotation curves of late-type galaxies are about constant to large radii, the masses can be estimated by measuring the rotation speed within the outer regions of the luminous galaxy component, which corresponds to the inner halo region (Sec. 4.1). Considering that the virial masses of the haloes in Miller et al. (2014) are converted from the inner circular velocity, $V_{2.2}$, of the galaxies, we now apply the same method to calculate the virial masses for the same galaxies in MOND. The total stellar masses, M_s , and $V_{2.2}$ are known in Miller et al. (2014), and they follow a simple fitting function (Miller et al. 2011, 2014)⁷,

$$\log_{10} \left(\frac{M_s}{M_\odot} \right) = [a + b \log_{10} \left(\frac{V_{2.2}}{\text{km s}^{-1}} \right)]. \quad (\text{B1})$$

Here $a = 0.57 \pm 0.48$ in M_s and $b = 4.35 \pm 0.62$. From Eq. 6 we know that $M_b = \frac{V_{200}^4}{G a_0}$. Thus for gas-poor galaxies, the relation is

$$\log_{10} \left(\frac{V_{200}^4}{G a_0} \right) = a + b \log_{10}(V_{2.2}); \quad (\text{B2})$$

while for gas-rich galaxies, $M_s = M_b/2 = \frac{V_{200}^4}{2G a_0}$, the relation is

$$\log_{10} \left(\frac{V_{200}^4}{2G a_0} \right) = a + b \log_{10}(V_{2.2}). \quad (\text{B3})$$

Combining with Eq. 19, the virial masses of the galaxies in the sample of Miller et al. (2014) are:

$$\log_{10} \left(\frac{M_{\text{vir}}}{h} \right) = \frac{3}{4} [a + b \log_{10}(V_{2.2}) + \log_{10}(a_0)], \quad (\text{gas-poor});$$

⁷ The last term on the right hand side of Eq. 5 in Miller et al. (2011) should not exist.

$$\log_{10} \left(\frac{M_{\text{vir}}}{h} \right) = \frac{3}{4} [a + b \log_{10}(V_{2.2}) + \log_{10}(2a_0)], \quad (\text{gas-rich}). \quad (\text{B4})$$

However, the fitting parameters for the Tully-Fisher relation introduced by Miller et al. (2011, 2014) are strongly sample-dependent, and the errors for $V_{2.2}$ are large and up to 60% (see Table 1 in Miller et al. 2014). Hence the virial masses calculated with Eq. B4 are unreliable. Thus we do not calculate the virial masses of the galaxies using Eq. 22 and we use Eq. B4 instead.

REFERENCES

Abadi M. G., Navarro J. F., Steinmetz M., Eke V. R., 2003, *ApJ*, 591, 499
 Aghertz O., Teyssier R., Moore B., 2011, *MNRAS*, 410, 1391
 Akerib D. S., Bai X., Bernard E., Bernstein A., Bradley A., Byram D., Cahn S. B., Carmona-Benitez M. C., et al. 2013, *Astroparticle Physics*, 45, 34
 Aumer M., White S. D. M., Naab T., Scannapieco C., 2013, *MNRAS*, 434, 3142
 Begeman K. G., Broeils A. H., Sanders R. H., 1991, *MNRAS*, 249, 523
 Behroozi P. S., Wechsler R. H., Conroy C., 2013, *ApJ*, 770, 57
 Bekenstein J., 2006, *Contemporary Physics*, 47, 387
 Bekenstein J., Milgrom M., 1984, *ApJ*, 286, 7
 Bekenstein J. D., 2004, *Phys. Rev. D*, 70, 083509
 Bhattacharyya G. K., Johnson Richard Arnold j. a., 1977, *Statistical concepts and methods* / Gouri K. Bhattacharyya, Richard A. Johnson. New York : John Wiley
 Bienaymé O., Famaey B., Wu X., Zhao H. S., Aubert D., 2009, *A&A*, 500, 801
 Blumenthal G. R., Faber S. M., Primack J. R., Rees M. J., 1984, *Nature*, 311, 517
 Bode P., Ostriker J. P., Turok N., 2001, *ApJ*, 556, 93
 Bosma A., 1981, *AJ*, 86, 1825
 Boylan-Kolchin M., Bullock J. S., Kaplinghat M., 2011, *MNRAS*, 415, L40
 Bruneton J.-P., Esposito-Farèse G., 2007, *Phys. Rev. D*, 76, 124012
 Bullock J. S., Johnston K. V., 2005, *ApJ*, 635, 931
 Colín P., Avila-Reese V., Valenzuela O., 2000, *ApJ*, 542, 622
 Collins M. L. M., Chapman S. C., Rich R. M., Irwin M. J., Peñarrubia J., Ibata R. A., Arimoto N., Brooks A. M., Ferguson A. M. N., Lewis G. F., McConnachie A. W., Venn K., 2011, *MNRAS*, 417, 1170
 Cox T. J., Loeb A., 2008, *MNRAS*, 386, 461
 Davis M., Efstathiou G., Frenk C. S., White S. D. M., 1985, *ApJ*, 292, 371
 Delgado-Serrano R., Hammer F., Yang Y. B., Puech M., Flores H., Rodrigues M., 2010, *A&A*, 509, A78
 Disney M. J., Romano J. D., Garcia-Appadoo D. A., West A. A., Dalcanton J. J., Cortese L., 2008, *Nature*, 455, 1082
 D’Onghia E., Burkert A., 2004, *ApJ*, 612, L13
 Eggen O. J., Lynden-Bell D., Sandage A. R., 1962, *ApJ*, 136, 748
 Einstein A., 1916, *Annalen der Physik*, 354, 769
 Fakhouri O., Ma C.-P., Boylan-Kolchin M., 2010, *MNRAS*, 406, 2267

Famaey B., Binney J., 2005, MNRAS, 363, 603

Famaey B., McGaugh S. S., 2012, Living Reviews in Relativity, 15, 10

Ferrero I., Abadi M. G., Navarro J. F., Sales L. V., Gurovich S., 2012, MNRAS, 425, 2817

Gao L., Theuns T., 2007, Science, 317, 1527

Gentile G., Famaey B., Combes F., Kroupa P., Zhao H. S., Tiret O., 2007, A&A, 472, L25

Gentile G., Famaey B., Zhao H., Salucci P., 2009, Nature, 461, 627

Governato F., Brook C., Mayer L., Brooks A., Rhee G., Wadsley J., Jonsson P., Willman B., Stinson G., Quinn T., Madau P., 2010, Nature, 463, 203

Guedes J., Callegari S., Madau P., Mayer L., 2011, ApJ, 742, 76

Guo Q., White S., Li C., Boylan-Kolchin M., 2010, MNRAS, 404, 1111

Halle A., Zhao H., Li B., 2008, ApJS, 177, 1

Helmi A., 2008, A&A Rev., 15, 145

Herpich J., Stinson G. S., Macciò A. V., Brook C., Wadsley J., Couchman H. M. P., Quinn T., 2013, ArXiv e-prints, astro-ph/1308.1088

Hummers C. B., Bryan G. L., 2012, ApJ, 749, 140

Ibata R. A., Ibata N. G., Lewis G. F., Martin N. F., Conn A., Elahi P., Arias V., Fernando N., 2014, ApJ, 784, L6

Kallivayalil N., van der Marel R. P., Alcock C., Axelrod T., Cook K. H., Drake A. J., Geha M., 2006, ApJ, 638, 772

Katz N., Gunn J. E., 1991, ApJ, 377, 365

Kautsch S. J., 2009, Astronomische Nachrichten, 330, 100

Kazantzidis S., Zentner A. R., Kravtsov A. V., Bullock J. S., Debattista V. P., 2009, ApJ, 700, 1896

Kent S. M., 1987, AJ, 93, 816

Klypin A., Kravtsov A. V., Valenzuela O., Prada F., 1999, ApJ, 522, 82

Kormendy J., Drory N., Bender R., Cornell M. E., 2010, ApJ, 723, 54

Kriek M., van Dokkum P. G., Labbé I., Franx M., Illingworth G. D., Marchesini D., Quadri R. F., 2009, ApJ, 700, 221

Kroupa P., 2012, Publications of the Astronomical Society of Australia, 29, 395

Kroupa P., 2014, Can. J. Phys., in press, (arXiv: 1406.4860)

Kroupa P., Famaey B., de Boer K. S., Dabringhausen J., Pawłowski M. S., Boily C. M., Jerjen H., Forbes D., Hensler G., Metz M., 2010, A&A, 523, A32

Lena D., Robinson A., Marconi A., Axon D. J., Capetti A., Merritt D., Batcheldor D., 2014, ApJ, in press, (arXiv: 1409.3976)

Lüghausen F., Famaey B., Kroupa P., Angus G., Combes F., Gentile G., Tiret O., Zhao H., 2013, MNRAS, 432, 2846

Marinacci F., Pakmor R., Springel V., 2013, ArXiv e-prints, astro-ph/1305.5360

McGaugh S. S., 2004, ApJ, 609, 652

McGaugh S. S., 2011, Physical Review Letters, 106, 121303

McGaugh S. S., 2012, AJ, 143, 40

McGaugh S. S., Schombert J. M., Bothun G. D., de Blok W. J. G., 2000, ApJ, 533, L99

Milgrom M., 1983a, ApJ, 270, 371

Milgrom M., 1983b, ApJ, 270, 384

Milgrom M., 1983c, ApJ, 270, 365

Milgrom M., 1988, ApJ, 333, 689

Milgrom M., 1989, Comments on Astrophysics, 13, 215

Milgrom M., 1999, Physics Letters A, 253, 273

Milgrom M., 2008, New Astronomy Reviews, 51, 906

Milgrom M., 2009a, Phys. Rev. D, 80, 123536

Milgrom M., 2009b, MNRAS, 398, 1023

Milgrom M., 2009c, ApJ, 698, 1630

Milgrom M., 2014a, MNRAS, 437, 2531

Milgrom M., 2014b, Can. J. Phys., in press, (arXiv: 1404.7661)

Milgrom M., Sanders R. H., 2003, ApJ, 599, L25

Miller S. H., Bundy K., Sullivan M., Ellis R. S., Treu T., 2011, ApJ, 741, 115

Miller S. H., Ellis R. S., Newman A. B., Benson A., 2014, ApJ, 782, 115

Moore B., Diemand J., Madau P., Zemp M., Stadel J., 2006, MNRAS, 368, 563

Moore B., Ghigna S., Governato F., Lake G., Quinn T., Stadel J., Tozzi P., 1999, ApJ, 524, L19

More S., van den Bosch F. C., Cacciato M., Mo H. J., Yang X., Li R., 2009, MNRAS, 392, 801

Naab T., Burkert A., 2003, ApJ, 597, 893

Navarro J. F., Benz W., 1991, ApJ, 380, 320

Navarro J. F., Steinmetz M., 1997, ApJ, 478, 13

Newman J. A., Cooper M. C., Davis M., Faber S. M., Coil A. L., Guhathakurta P., Koo D. C., Phillips A. C., et al. 2013, ApJS, 208, 5

Okamoto T., Eke V. R., Frenk C. S., Jenkins A., 2005, MNRAS, 363, 1299

Pawlowski M. S., Famaey B., Jerjen H., Merritt D., Kroupa P., Dabringhausen J., Lüghausen F., Forbes D. A., Hensler G., Hammer F., Puech M., Fouquet S., Flores H., Yang Y., 2014, MNRAS, 442, 2362

Piontek F., Steinmetz M., 2011, MNRAS, 410, 2625

Planck M., 1901, Annalen der Physik, 309, 564

Reyes R., Mandelbaum R., Gunn J. E., Nakajima R., Seljak U., Hirata C. M., 2012, MNRAS, 425, 2610

Rubin V. C., Burstein D., Ford Jr. W. K., Thonnard N., 1985, ApJ, 289, 81

Rubin V. C., Ford Jr. W. K., 1970, ApJ, 159, 379

Rubin V. C., Ford Jr. W. K., Thonnard N., Burstein D., 1982, ApJ, 261, 439

Samland M., Gerhard O. E., 2003, A&A, 399, 961

Sanders R. H., 1990, A&A Rev., 2, 1

Sanders R. H., 2005, MNRAS, 363, 459

Sanders R. H., 2009, Advances in Astronomy, 2009, 752439

Sanders R. H., McGaugh S. S., 2002, ARA&A, 40, 263

Sanders R. H., Noordermeer E., 2007, MNRAS, 379, 702

Scannapieco C., Wadepluh M., Parry O. H., Navarro J. F., Jenkins A., Springel V., Teyssier R., Carlson E., et al. 2012, MNRAS, 423, 1726

Scarpa R., 2006, in Lerner E. J., Almeida J. B., eds, First Crisis in Cosmology Conference Vol. 822 of American Institute of Physics Conference Series, Modified Newtonian Dynamics, an Introductory Review. pp 253–265

Schaye J., Crain R. A., Bower R. G., Furlong M., Schaller M., Theuns T., Dalla Vecchia C., Frenk C. S., et al. 2014, MNRAS, in press, (arXiv: 1407.7040)

Schneider A., Smith R. E., Macciò A. V., Moore B., 2012, MNRAS, 424, 684

Skordis C., 2008, Phys. Rev. D, 77, 123502

Skordis C., Zlosnik T., 2012, Phys. Rev. D, 85, 044044

Sommer-Larsen J., Götz M., Portinari L., 2003, ApJ, 596,

47

Springel V., Wang J., Vogelsberger M., Ludlow A., Jenkins A., Helmi A., Navarro J. F., Frenk C. S., White S. D. M., 2008, MNRAS, 391, 1685

Stewart K. R., Bullock J. S., Wechsler R. H., Maller A. H., Zentner A. R., 2008, ApJ, 683, 597

Stinson G. S., Brook C., Macciò A. V., Wadsley J., Quinn T. R., Couchman H. M. P., 2013, MNRAS, 428, 129

Tiret O., Combes F., 2009, A&A, 496, 659

Toomre A., 1977, in Tinsley B. M., Larson D. Campbell R. B. G., eds, Evolution of Galaxies and Stellar Populations Mergers and Some Consequences. p. 401

Trippé S., 2013, Journal of Korean Astronomical Society, 46, 133

Tully R. B., Fisher J. R., 1977, A&A, 54, 661

Vogelsberger M., Genel S., Springel V., Torrey P., Sijacki D., Xu D., Snyder G., Nelson D., Hernquist L., 2014, MNRAS, 444, 1518

Walker I. R., Mihos J. C., Hernquist L., 1996, ApJ, 460, 121

Weil M. L., Eke V. R., Efstathiou G., 1998, MNRAS, 300, 773

Wilcoxon F., 1945, Biometrics Bulletin, 1, 80

Wu X., Famaey B., Gentile G., Perets H., Zhao H., 2008, MNRAS, 386, 2199

Wu X., Kroupa P., 2013, MNRAS, 435, 1536

Younger J. D., Cox T. J., Seth A. C., Hernquist L., 2007, ApJ, 670, 269

Zhao H., 2007, ApJ, 671, L1

Zhao H. S., 2008, Modern Physics Letters A, 23, 555

Zhao H. S., Tian L., 2006, A&A, 450, 1005

Zlosnik T. G., Ferreira P. G., Starkman G. D., 2007, Phys. Rev. D, 75, 044017